

## **Title**

A native prokaryotic voltage-dependent calcium channel with a novel selectivity filter sequence

## **Authors**

Takushi Shimomura<sup>1,3</sup>, Yoshiki Yonekawa<sup>2</sup>, Hitoshi Nagura<sup>1</sup>, Michihiro Tateyama<sup>3</sup>, Yoshinori Fujiyoshi<sup>1‡,4</sup> and Katsumasa Irie<sup>1,2</sup>.

<sup>1</sup>Cellular and Structural Physiology Institute (CeSPI), and <sup>2</sup>Graduate School of Pharmaceutical Sciences, Nagoya University, Furo-cho, Chikusa, Nagoya 464-8601, Japan.

<sup>3</sup>Division of Biophysics and Neurobiology, National Institute for Physiological Sciences, Okazaki, Aichi, 444-8585, Japan

<sup>4</sup>CeSPIA Inc., 2-1-1, Otemachi, Chiyoda, Tokyo, 100-0004, Japan

‡present address: Advanced Research Institute, Tokyo Medical and Dental University, 1-5-45 Yushima, Bunkyo-ku, Tokyo 113 - 8510, Japan

Address correspondence to: Katsumasa Irie, Cellular and Structural Physiology Institute (CeSPI), Nagoya University, Furo-cho, Chikusa, Nagoya 464-8601, Japan Tel.: +81-52-747-6838; Fax: +81-52-747-6795; E-mail: [kirie@cespi.nagoya-u.ac.jp](mailto:kirie@cespi.nagoya-u.ac.jp)

## Abstract

Voltage-dependent  $\text{Ca}^{2+}$  channels (Cavs) are indispensable for coupling action potentials with  $\text{Ca}^{2+}$  signaling in living organisms. The structure of Cavs is similar to that of voltage-dependent  $\text{Na}^{+}$  channels (Navs). It is known that prokaryotic Navs can obtain  $\text{Ca}^{2+}$  selectivity by negative charge mutations of the selectivity filter, but native prokaryotic Cavs had not yet been identified.

Here, we report the first identification of a native prokaryotic Cav, CavMr, and its relative, NavPp. Although CavMr contains a smaller number of negatively charged residues in the selectivity filter than artificial prokaryotic Cavs, CavMr exhibits high  $\text{Ca}^{2+}$  selectivity. In contrast, NavPp, which has similar filter sequence to artificial Cavs, mainly allows  $\text{Na}^{+}$  to permeate. Interestingly, a NavPp mutant whose selectivity filter was replaced with that of CavMr exhibits high  $\text{Ca}^{2+}$  selectivity. Mutational analyses revealed that the glycine residue of the CavMr selectivity filter is a determinant for  $\text{Ca}^{2+}$  selectivity. This glycine residue is well conserved among subdomains I and III of eukaryotic Cavs.

These findings provide new insight into the  $\text{Ca}^{2+}$  selectivity mechanism conserved from prokaryotes to eukaryotes.

### **Significance Statement**

CavMr is the first identified native prokaryotic Cav. CavMr has a unique selectivity filter sequence different from that of artificial prokaryotic Cavs derived from canonical prokaryotic Navs. Unlike artificial Cavs, the glycine residue of the selectivity filter of CavMr is important for the selective permeation of  $\text{Ca}^{2+}$  ions, indicating that there are two different mechanisms of  $\text{Ca}^{2+}$  recognition. Interestingly, corresponding glycine residues are found in subdomains I and III of eukaryotic Cavs.

These findings suggest that the small glycine residue in the Cav selectivity filter is an overlooked feature determining  $\text{Ca}^{2+}$  selectivity. Therefore, further investigation of CavMr will contribute to our understanding of the principles underlying  $\text{Ca}^{2+}$  selectivity.

## Introduction

Voltage-dependent  $\text{Ca}^{2+}$  channels (Cavs), which couple the membrane voltage with  $\text{Ca}^{2+}$  signaling, regulate some important physiological functions, such as neurotransmission and muscle contraction (1). The channel subunits of mammalian Cavs as well as mammalian voltage-dependent  $\text{Na}^+$  channels (Navs) have 24 transmembrane helices (24TM) (2), and comprise 4 homologous subdomains with 6 transmembrane helices that correspond to one subunit of homo-tetrameric channels, such as Kvs and prokaryotic Navs (BacNavs). Comparison of the sequences between Navs and Cavs indicate that Navs derived from Cavs. Their two pairs of subdomains, domains I and III, and domains II and IV, are evolutionarily close to each other (3, 4). Therefore, the 24TM-type of Cavs are thought to have evolved from the single-domain type of Cavs with two times of domain duplications. Although prokaryotes are expected to have such ancestor-like channels, native prokaryotic Cavs have not yet been identified. The lack of ancestor-like prokaryotic Cavs is a missing link in the evolution of voltage-dependent cation channels.

In contrast to the lack of prokaryotic Cavs, many BacNavs have been characterized (5–12). The simple structure of BacNavs has helped to elucidate the molecular mechanisms of Nav (13–16). In addition to this point, BacNavs has been used as the genetic tool for manipulating the neuronal excitability in vivo (17–19). The introduction of a several negatively charged amino acids into the selectivity filter of BacNavs leads to the acquisition of  $\text{Ca}^{2+}$  selectivity (16, 20). Such a mutant of NavAb (a BacNav from *Arcobacter butzleri*) showed high  $\text{Ca}^{2+}$  selectivity, and the structural basis of  $\text{Ca}^{2+}$  selectivity has been discussed on the basis of its crystal structures (20, 21). The selectivity filter sequences with a large number of aspartates in CavAb, which was made by mutations of NavAb, are quite different from those of the original mammalian Cavs.

Here, we newly characterized two BacNav homologues, CavMr from *Meiothermus ruber* and NavPp from *Plesiocystis pacifica*. These two channels are evolutionarily distant from the previously reported canonical BacNavs. We confirmed that CavMr has clear  $\text{Ca}^{2+}$  selectivity, and NavPp has  $\text{Na}^+$  selectivity with  $\text{Ca}^{2+}$ -dependent inhibition. The discovery of these channels suggests the possible importance of voltage-regulated  $\text{Ca}^{2+}$  signaling in prokaryotes and may be a new genetic tool for controlling  $\text{Ca}^{2+}$  signaling. Furthermore, mutational analyses indicate that the glycine residue of the CavMr selectivity filter is important for  $\text{Ca}^{2+}$  selectivity. The glycine residue is also well conserved in the selectivity filter of the subdomain I and III of mammalian Cavs. On the basis of these observations, we propose that CavMr is an ancestral-type of native prokaryotic Cav with a  $\text{Ca}^{2+}$  selectivity mechanism different from that in artificial

CavAb. CavMr and NavPp are expected to advance our understanding of  $\text{Ca}^{2+}$  recognition and the evolution of voltage-dependent cation channels.

## Results

### **Identification of two prokaryotic channels with $\text{Ca}^{2+}$ permeability and inhibition.**

We searched for the primary sequences of prokaryotic Cavs in the GenBank<sup>TM</sup> database. In mammalian and prokaryotic Navs and Cavs, a larger number of negative charges in the filter increases  $\text{Ca}^{2+}$  selectivity (16, 22, 23). Several BLAST search rounds using the pore regions (S5-S6) of NaChBac (or NavBh; a BacNav from *Bacillus halodurans*) as templates revealed a series of candidate prokaryotic Cavs (Fig.1a) with a selectivity filter sequence similar to the “TLESW” motif, but more negatively charged: ZP\_04038264 from *Meiothermus ruber*, ZP\_01909854 from *Plesiocystis pacifica*, YP\_003896792\_from *Halomonas elongata*, and YP\_003073405 from *Teredinibacter turnerae* (SI Appendix, Fig.S1a). These channels belong to a different branch of the phylogenetic tree than that of canonical BacNavs (Fig.1a) and have some negatively charged residues in their selectivity filter, similar to CavAb (Fig.1b). In the case of the expression of prokaryotic channels, insect cells are better than mammalian cells to generate large current amplitudes (13). We therefore transfected Sf9 cells with these genes and measured the resulting whole-cell currents. Although the cells transfected with genes from *H. elongata* and *T. turnerae* failed to show detectable currents, those from *M. ruber* and *P. pacifica* showed currents in response to a depolarizing stimulus from a -140 mV holding potential (Fig.1c and d). To estimate the  $\text{Ca}^{2+}$  permeability, we measured their current-voltage relationships. The *M. ruber* channel had clearly larger currents in the high- $\text{Ca}^{2+}$  solution than in the high- $\text{Na}^+$  solution, and very positive reversal potential was observed in a high- $\text{Ca}^{2+}$  bath solution (Fig.1e). In contrast, the currents derived from the *P. pacifica* channel increased with increases in the bath  $\text{Na}^+$  concentration and significantly decreased when the  $\text{Na}^+$  solution was replaced with a high  $\text{Ca}^{2+}$  solution. The reversal potential fit well to the  $\text{Na}^+$  equilibrium potential in the high- $\text{Na}^+$  solution (Fig.1f). These current-voltage relationships suggest that the *M. ruber* channel has a preference for  $\text{Ca}^{2+}$  and the *P. pacifica* channel has a preference for  $\text{Na}^+$ . Therefore, the two newly identified channels from *M. ruber* and *P. pacifica* are abbreviated as CavMr and NavPp respectively, based on their ion selectivity and species name.

To clearly compare the positions of the residues in the selectivity filter in each channel, we renumbered the seven residues comprising the selectivity filter in the following description. For example, the seven residues of the CavMr selectivity filter are

183-TLEGWVD-189, and thus Thr183 and Asp189 were renumbered to Thr1 and Asp7 (Fig.1b). Notably, the amino acid sequence of the selectivity filter in CavMr is similar to the conserved features of domains I/III in mammalian Caves, a glycine at position 4 and a polar or negatively charged residue at position 7 (Fig.1b), which are not observed in the BacNav family. In addition, its sequence is quite similar to that of the human Cav subdomain I, or even the same as Cav3.1 and 3.2 (Fig.1b).

In the following experiments, to accurately evaluate the reversal potential for the ion selectivity analysis, we introduced a single mutation that resulted in large and long-lasting channel currents. T220A and G229A mutations in NaChBac led to slower inactivation, indicating suppression of the transition to the inactivated state (8, 9). We introduced a T232A mutation to NavPp and a G240A mutation to CavMr, corresponding to the NaChBac mutations of T220A and G229A, respectively. These mutants stably showed measurable currents, even after they were administered multiple depolarizing stimuli (*SI Appendix*, Fig.S1b-e).

### **CavMr has high Ca<sup>2+</sup> selectivity over Na<sup>+</sup>.**

We accurately quantified the selectivity of CavMr for Na<sup>+</sup> and Ca<sup>2+</sup> ( $P_{Ca}/P_{Na}$ ) by measuring the reversal potential under bi-ionic conditions, in which the Ca<sup>2+</sup> concentration in the bath solution was changed to 1.5, 4, 10, 20, and 40 mM while the intracellular Na<sup>+</sup> concentration was held constant at 150 mM (Fig.2a and b). The plot of the reversal potentials as a function of [Ca<sup>2+</sup>] had a slope of  $41.07 \pm 2.64$  mV /decade ( $n = 4$ ), a value close to that for Ca<sup>2+</sup> (Fig. 2c), and indicated that CavMr had a  $P_{Ca}/P_{Na}$  of  $218 \pm 38$  (Fig.2a and b, Table1). This high  $P_{Ca}/P_{Na}$  value is comparable to that of CavAb. Among several species of cations, including Sr<sup>2+</sup>, K<sup>+</sup>, and Cs<sup>+</sup> (Fig.2d and e), Ca<sup>2+</sup> had the highest permeability relative to Na<sup>+</sup> (Fig.2f and g, Table1). On the basis of these results, CavMr was confirmed to be a native prokaryotic Cav with high Ca<sup>2+</sup> selectivity. We also investigated whether CavMr shows the typical anomalous mole fraction effect (24) and the non-monotonic mole fraction effect observed in NaChBac (25). CavMr did not allow Na<sup>+</sup> permeation under Ca<sup>2+</sup>-free (0 mM CaCl<sub>2</sub> and 1 mM EGTA) conditions (*SI Appendix*, Fig. S2a and b). Also, different from the recording of NaChBac currents in a solution containing Na<sup>+</sup> and K<sup>+</sup>, CavMr had an apparently monotonic current increase depending on the Ca<sup>2+</sup> mole fraction to Na<sup>+</sup> (*SI Appendix*, Fig. S2c and d).

Studies of an artificial Cav, CavAb, revealed that Ca<sup>2+</sup> selectivity depends on a large number of aspartates in the filter sequence (20). The high Ca<sup>2+</sup> selectivity in CavMr was unexpected because the filter sequence contained only one aspartate residue (Fig.1b). Furthermore, CavMr-D7M, which has only one negatively charged residue in the

selectivity filter “TLEGWVM”, still had high  $\text{Ca}^{2+}$  selectivity comparable to that of wild-type CavMr ( $P_{\text{Ca}}/P_{\text{Na}} = 144 \pm 12$ ; *SI Appendix*, Fig. S2e and f and Table1). These findings indicate that CavMr and artificial CavAb have different  $\text{Ca}^{2+}$  selective mechanisms.

### **NavPp is permeable to $\text{Na}^+$ and is blocked by extracellular $\text{Ca}^{2+}$ .**

The current-voltage relationships of NavPp revealed a preference for  $\text{Na}^+$  (Fig.1d and f). Interestingly, NavPp, although having one more aspartate in the selectivity filter than CavMr, exhibited larger currents in  $\text{Na}^+$  solutions than in  $\text{Ca}^{2+}$  solutions (Fig.1b and d). Recordings in bath solution containing both  $\text{Na}^+$  and  $\text{Ca}^{2+}$  demonstrated that increasing the extracellular  $\text{Ca}^{2+}$  decreased the current in NavPp and led to a positive shift in the voltage dependence, indicating that a higher concentration of  $\text{Ca}^{2+}$  inhibited NavPp (Fig.1f and Fig. 3a and *SI Appendix*, Fig. S3a). With NavAb, increasing the  $\text{Ca}^{2+}$  concentration with a constant  $\text{Na}^+$  concentration in the bath solution led to a small increase in the current amplitude, probably due in part to  $\text{Ca}^{2+}$  permeability (Fig. 3a and *SI Appendix*, Fig. S3b). We also investigated the dependence of the direction of current flow on  $\text{Ca}^{2+}$  inhibition by comparing pipette solutions containing 10 mM or 150 mM  $\text{Na}^+$ , in which the current flowed in an inward or outward direction, respectively, even under the same -10 - mV depolarizing stimulus (Fig. 3a and *SI Appendix*, Fig. S3a and c). The results demonstrated that the inhibitory effects of  $\text{Ca}^{2+}$  on NavPp were independent of the current direction.

We then compared the relative permeability of various cations with that of  $\text{Na}^+$  in NavPp. In bi-ionic conditions with high concentration of  $\text{Ca}^{2+}$  in the bath and high  $\text{Na}^+$  in the pipette, the outward current was completely blocked by  $\text{Ca}^{2+}$  (Fig. 3a), and the inward current was hardly observed. The reversal potential was obtained under an extracellular solution containing  $\text{Na}^+$  ions, however, despite a partial  $\text{Ca}^{2+}$  or  $\text{Sr}^{2+}$ -induced block (Fig. 3b and c). The selectivity of NavPp was higher for  $\text{Na}^+$  than for  $\text{Ca}^{2+}$ ,  $\text{Sr}^{2+}$ ,  $\text{K}^+$ , and  $\text{Cs}^+$  (Fig. 3d and *SI Appendix*, Fig. S3d and e). The  $P_{\text{Ca}}/P_{\text{Na}}$  was  $0.308 \pm 0.028$  in a bath solution containing both  $\text{Ca}^{2+}$  and  $\text{Na}^+$ , suggesting that a larger fraction of  $\text{Ca}^{2+}$  is allowed to permeate with outside  $\text{Na}^+$  ions through NavPp than through canonical BacNavs. Similar to  $\text{Ca}^{2+}$ ,  $\text{Sr}^{2+}$  also blocked the NavPp current, but may also permeate the channel along with  $\text{Na}^+$  ions (Fig. 3c). These findings demonstrate a unique feature of NavPp, a low affinity  $\text{Ca}^{2+}$  block, which is not reported in canonical BacNavs.

Interestingly, the filter sequence of NavPp, "TLEDWTD", has three negatively-charged residues, similar to the filter sequences of the artificial

Ca<sup>2+</sup>-selective BacNav mutants ( “TLEDWSD” mutant of NavAb and ”TLEDWAD” mutant of NaChBac ) (16, 20). NavPp does not show Ca<sup>2+</sup> permeability, however, but rather a Ca<sup>2+</sup> block. We also investigated NavPp mutants with the same filter sequences as the artificial CavMs. NavPp-T6S “TLEDWSD” exhibited Ca<sup>2+</sup>-blocked currents similar to wild-type NavPp (*SI Appendix*, Fig. S3f). Further, NavPp-T6A “TLEDWAD” showed no inward current in bath solutions containing divalent cations, suggesting that the Ca<sup>2+</sup>-induced block was enforced. Therefore, both of the selectivity filter sequences providing Ca<sup>2+</sup> selectivity to canonical BacNavs failed to generate Ca<sup>2+</sup>-permeable NavPp, indicating that the cation permeable mechanism of NavPp differs from that of canonical BacNavs, as well as that of CavMr.

### **Swapping the filter regions between CavMr and NavPp revealed the importance of the glycine residue at position 4 for Ca<sup>2+</sup> selective permeation.**

To search for the determinants of Ca<sup>2+</sup> selectivity in CavMr, we investigated a series of mutants in which the filter regions were swapped between CavMr and NavPp (Fig. 4a and b). The mutants with filter sequences swapped between NavPp and CavMr exhibited channel activity (*SI Appendix*, Fig. S4). A NavPp mutant whose selectivity filter was replaced with that of CavMr, named NavPp-Mr, exhibited much higher Ca<sup>2+</sup> selectivity ( $P_{Ca}/P_{Na} = 215 \pm 33$ ) as well as high Sr<sup>2+</sup> selectivity, comparable to that of CavMr (Fig. 4c). In addition, NavPp-Mr excluded Cs<sup>+</sup> similar to CavMr, but weakly allowed K<sup>+</sup> permeation in contrast to CavMr. On the other hand, a CavMr mutant whose selectivity filter was replaced with that of NavPp (CavMr-Pp) almost lost its Ca<sup>2+</sup> selectivity ( $P_{Ca}/P_{Na} = 13.8 \pm 2.0$ ), and was less able to discriminate Cs<sup>+</sup> and K<sup>+</sup> from Na<sup>+</sup> (Fig. 4d). That is, CavMr-Pp was a more non-selective channel than the wild-type CavMr, rather than a Na<sup>+</sup>-selective channel. Namely, the Ca<sup>2+</sup> selectivity (from NavPp to CavMr) was almost transferable, but the Na<sup>+</sup> selectivity was not. We also investigated the full swapping of the filter sequences between CavMr and NavAb (Fig. 4a), but neither swapped mutant of CavMr and NavAb had detectable currents. This finding suggested that CavMr and NavAb achieve cation selectivity by different structural backbones and mechanisms.

Positions 4 and/or 6 of the filter sequences are thought to be important for Ca<sup>2+</sup>-selective permeation in NavPp-Mr and CavMr, because only these two positions were mutated in the swapping experiments. We investigated which of the mutations in positions 4 and 6 had greater effects on the loss of and acquisition of Ca<sup>2+</sup> selectivity in CavMr and NavPp, respectively. In CavMr, both of two single mutants, CavMr-G4D and CavMr-V6T, decreased Ca<sup>2+</sup> selectivity and allowed K<sup>+</sup> and Cs<sup>+</sup> permeation (Fig. 5a,



*SI Appendix*, Fig.S5). Especially, the mutational effect was greater in CavMr-G4D, whose  $P_{Ca}/P_{Na}$  was less than 10 ( $7.73 \pm 2.24$ ). CavMr-G4S, in which Gly4 was replaced with the Ser4 of NavAb, also exhibited lower  $Ca^{2+}$  selectivity ( $P_{Ca}/P_{Na} = 11.9 \pm 1.5$ ) and was also  $K^+$  and  $Cs^+$  permeable, indicating that even a minor substitution by serine is not tolerable and does not allow for the selection of specific cations (Fig. 5b, Table1, and *SI Appendix*, Fig. S6). In the case of NavPp, NavPp-D4G acquired  $Ca^{2+}$  selectivity over  $Na^+$ , and also showed a greater exclusion to  $K^+$  and  $Cs^+$  than wild-type NavPp (Fig. 5c and *SI Appendix*, Fig.S5). In contrast, NavPp-T6V failed to acquire the high  $Ca^{2+}$  selectivity ( $P_{Ca}/P_{Na} = 1.72 \pm 1.09$ ) and also allowed  $K^+$  and  $Cs^+$  permeation, while it had relatively high  $Sr^{2+}$  selectivity. These results indicate that, in both CavMr and NavPp, a glycine residue at position 4 is a key determinant for  $Ca^{2+}$  selectivity. It is noteworthy that the glycine is a conserved residue at position 4 of subdomains I and III in all subtypes of mammalian Cavs (Fig.1b).

## DISCUSSION

### **A native prokaryotic voltage-dependent $Ca^{2+}$ channel has a unique $Ca^{2+}$ selective mechanism.**

In this study, we newly characterized two prokaryotic voltage-dependent cation channels, CavMr and NavPp. CavMr is the first native prokaryotic Cavs reported despite its BacNav-like “TxExW” motif, and NavPp could be inhibited by high concentrations of extracellular  $Ca^{2+}$ . The  $P_{Ca}/P_{Na}$  of CavMr was more than 200 (Fig. 2e and Table 1), comparable to that of CavAb, an artificial  $Ca^{2+}$  channel. Anomalous mole fraction effects were not observed in CavMr (*SI Appendix*, Fig. S2a and b), suggesting that CavMr has a very high affinity for  $Ca^{2+}$ . In addition to providing new insights about general  $Ca^{2+}$ -selective mechanisms, CavMr has the potential to be a new genetic tool for upregulating calcium signaling, as BacNavs are useful genetic tools for increasing action potential firing in mice (17–19).

Phylogenetic analysis demonstrated that CavMr and NavPp are similar to each other, but distant from canonical BacNavs (Fig. 1a). The high  $Ca^{2+}$  selectivity of CavMr was transferable to NavPp. Intriguingly, two pairs of mutants with the same selectivity filter (CavMr-G4D and NavPp-T6V, CavMr-V6T and NavPp-D4G) showed a very similar tendency with regard to both the order and extent of cation selectivity (Fig. 5a and c). Therefore, the basic overall architecture of the NavPp selectivity filter could be similar to that of CavMr. On the other hand, the  $Ca^{2+}$  selectivity mechanism of CavMr completely differs from that of CavAb. Structural comparison of NavAb and CavAb showed that the aspartate mutations did not alter the main chain trace, and simply

introduced the negative charges around the ion pathway to increase  $\text{Ca}^{2+}$  permeability (Fig. 7a and b) (20). In contrast, in the case of CavMr, two non-charged residues (Gly4 and Val6) are required for the high  $\text{Ca}^{2+}$  selectivity (Fig. 4c, 5a), but Asp7 is not necessary (*SI Appendix*, Fig. S2f). A no-charge mutation at position 7, CavMr-D7M “TLEGWVM”, is an outstanding example demonstrating that high  $\text{Ca}^{2+}$  selectivity can be achieved in the absence of any aspartates in its filter region (*SI Appendix*, Fig. S2f). Furthermore, the introduction of a negative charge into the selectivity filter (G4D mutation) had the opposite effect on the  $\text{Ca}^{2+}$  selectivity of CavMr compared with NavAb and NaChBac (16, 22). Moreover, the decreased selectivity in G4S also indicates that the glycine at position 4 is indispensable for  $\text{Ca}^{2+}$  selectivity in CavMr (Fig. 5b). The flexibility and/or small size of the glycine at position 4 in CavMr might be critical. These findings are inconsistent with the notion derived from the  $\text{Ca}^{2+}$ -selective mutants of NavAb and NaChBac, and therefore the native structure of the selectivity filter and the molecular mechanism of ion selectivity of CavMr are thought to differ from those of CavAb. While the structure of CavMr is not yet available, we are able to speculate on the structure of the selectivity filter of CavMr on the basis of the structure of human Cav1.1 subdomains I and III (26) (Fig. 6c), whose selectivity filter sequences are very similar to that of CavMr. In the selectivity filter of Cav1.1 subdomains I and III, the side chain of the residue at position 7 is shifted outward. The position-4 glycine residue widens the entrance of the selectivity filter, which would facilitate the entry of hydrated cations into the ion pore and might increase  $\text{Ca}^{2+}$  selectivity.

### **Cavs in prokaryotes and the species-specific tuning of homo-tetrameric channels.**

Prokaryotes have a number of putative  $\text{Ca}^{2+}$  binding proteins, such as EF-hand proteins, P-type  $\text{Ca}^{2+}$  pumps, and  $\text{Ca}^{2+}$  transporters (27). The intracellular  $\text{Ca}^{2+}$  concentration is kept low and changes in response to mechanical and chemical stimuli (28). These features imply that prokaryotic  $\text{Ca}^{2+}$  signaling is similar to that of eukaryotes. The strong ability of CavMr to exclude  $\text{Na}^+$  and  $\text{K}^+$  along with  $\text{Ca}^{2+}$  permeation suggests that its primary physiological role is  $\text{Ca}^{2+}$  intake in response to a voltage change (Fig. 2f and g). In some bacteria, the direction of flagellar rotation and chemotaxis changes depending on the internal  $\text{Ca}^{2+}$  concentration (29–31). *M. ruber* was isolated from hot springs, and therefore a sufficient amount of  $\text{Ca}^{2+}$  is likely to exist in its native environment (32). CavMr activation by a voltage change, which could vary depending on the environmental ionic conditions, might lead to any response to adapt to the new environment, such as flagellar rotation. These characteristics indicate the existence of

signal coupling between the membrane voltage and  $\text{Ca}^{2+}$ , even in the early stages of life, which might be the origin of the corresponding functions in eukaryotes, such as muscle contraction.

NavPp permeates more  $\text{Na}^+$  than  $\text{Ca}^{2+}$ , but its selectivity is modest (Fig. 3f and Table 1). Notably, *P. pacifica* is a marine myxobacterium that requires NaCl for its growth (33). As mentioned above, the basic architecture of the CavMr/NavPp group is thought to produce a preference for  $\text{Ca}^{2+}$ . *P. pacifica* might modify this channel architecture to acquire a  $\text{Na}^+$  intake pathway, which would likely result in the remaining feature of low-affinity  $\text{Ca}^{2+}$  inhibition in NavPp. This flexible usage of homo-tetrameric channels to allow different cations to permeate is also reported in another bacterium, *Bacillus alkalophilus* (34). NsvBa from *B. alkalophilus* is a non-selective channel whose selectivity filter is changed from “TLESWAS”, a typical  $\text{Na}^+$ -selective sequence in alkaliphilic bacillus, to “TLDSWGS”, possibly to adapt to its ionic environment. Recently, an early eukaryote, diatom, was found to have another homo-tetrameric channel with no selectivity that has an important role in electrical signaling in this species (35). These findings suggest that the cation selectivity of the homo-tetrameric channel family can be flexibly tuned to realize the required roles specific to its original species. We also found four homologues that have filter sequences similar to CavMr “Tx(E/D)GWx(D/E)” in the NCBI database (WP\_009945599.1, WP\_012983075.1, WP\_024079824.1, and XP\_002186055.1). XP\_002186055.1 belongs to diatoms, which implies the wide use of monomeric Cavs in various organisms – not only prokaryotes, but also eukaryotes.

### **Insights into $\text{Ca}^{2+}$ selectivity and the evolution of mammalian Cavs.**

Aspartate residues are generally observed in the  $\text{Ca}^{2+}$  permeation pathway in ion channels, as well as many  $\text{Ca}^{2+}$  binding proteins (36–38). Actually, NavAb and NaChBac were successfully transformed to  $\text{Ca}^{2+}$ -selective channels with the aspartate-introduced filter sequences “TLDDW(S/A)D” (16, 22). But, our results elucidate that this strategy is not the only method for achieving high  $\text{Ca}^{2+}$  selectivity. Human Cavs subdomains possess, at most, two aspartate residues in the selectivity filters in other part than position 3. In addition, the negatively charged residue at position 3, which is thought to be the most critical for cation selectivity in both Navs and Cavs, is not aspartate, but glutamate in most of the human Cavs subdomains (39). CavAb has 12 aspartates in the selectivity filter of a channel tetramer, while there are 4 aspartates in CavMr. The net negative charge is 5~7 in mammalian Cavs, 8 in CavMr, and 12 in CavAb. These findings indicate that  $\text{Ca}^{2+}$  selectivity can be achieved with

even fewer negative charges than CavAb and close to mammalian Cav, probably with the contribution of a special backbone structure around the selectivity filters.

It is noteworthy that the selectivity filter sequence of CavMr is very similar to those of human Cav subdomains I and III, both of which possess a glycine at position 4 (Fig. 6c). Especially, the Cav3.1 and 3.2 subdomains I have the same sequence as CavMr. On the other hand, the sequences of subdomains II and IV are relatively similar to that of CavAb (Fig. 6d). These sequence similarities of the glycine residue at position 4 are also found in CatSper, the sperm calcium permeable channel (40). The channel region of CatSper is formed by four different subunits (CatSper1-4). The selectivity filters of CatSper 3 “TVDGWTD” and CatSper 4 “TQDGWVD” are similar to that of CavMr and share a glycine residue at position 4 as well as subdomains I and III of 24TM Cavs. These similarities indicate the generality of the CavMr-like Ca<sup>2+</sup>-selectivity mechanism. Further investigation of the detailed structure of CavMr may help to elucidate the principles and origin underlying Ca<sup>2+</sup> selectivity.

## **Material and methods**

### **Cloning of BacNav homologues and site-directed mutagenesis**

The NaChBac amino acid sequence (NP\_242367) was used as the query for a BLASTP search against the Microbial Genomic database at NCBI. The identified primary sequence data were obtained from Entrez at NCBI (*Meiothermus ruber* as ZP\_04038264, *Plesiocystis pacifica* as ZP\_01909854, *Halomonas elongata* as YP\_003896792 and *Teredinibacter turnerae* as YP\_003073405). These DNAs were synthesized by Genscript Inc. and subcloned into the pCI vector (Promega) using the EcoRI and Sall sites and the pBiEX vector (Novagen) using NcoI and BamHI sites, respectively. Site-directed mutagenesis was achieved by polymerase chain reaction (PCR) of the full-length plasmid containing the Nav gene using PrimeSTAR<sup>®</sup> MAX DNA Polymerase (Takara Bio.). All clones were confirmed by DNA sequencing.

### **Electrophysiological analysis using mammalian cells**

For the recordings related to mole fraction effects (Fig. S2a-d), currents were recorded from Chinese hamster ovary (CHO) -K1 cells expressing channels. The recordings were performed as described previously (41). Cells were transfected with channel DNAs using the LipofectAMINE 2000 (Invitrogen) and plated onto cover slips. Currents were recorded 24-36 h after transfection. Current recording by the whole cell patch clamp technique was performed using Axopatch 200B amplifiers, Digidata1332A, and pClamp 9 software (Molecular Devices). The pipette solution contained 130 mM KCl, 5 mM Na<sub>2</sub>-ATP, 3 mM EGTA, 0.1 mM CaCl<sub>2</sub>, 4 mM MgCl<sub>2</sub> and 10 mM HEPES (pH 7.2 adjusted with KOH). The bath solution contained 135 mM NaCl, 4 mM KCl, 1 mM CaCl<sub>2</sub>, 5 mM MgCl<sub>2</sub> and 10 mM HEPES (pH 7.4 adjusted with NaOH). For the measurement of mole fraction effects, the bath solutions containing different ratio of NaCl / CaCl<sub>2</sub> (135/0, 108/18, 81/36, 54/54, 27/82 and 0/90 mM) were used. The Ca<sup>2+</sup>-free solution was achieved with the solution containing 135 mM NaCl, 1 mM EGTA and 0 mM CaCl<sub>2</sub>.

### **Electrophysiological measurement in insect cells**

The recordings other than those for mole fraction effects were performed using SF-9 cells. SF-9 cells were grown in Sf-900<sup>TM</sup> III medium (Gibco) complemented with 0.5% 100× Antibiotic-Antimycotic (Gibco) at 27°C. Cells were transfected with target channel-cloned pBiEX vectors and enhanced green fluorescent protein (EGFP)-cloned pBiEX vectors using Fugene HD transfection reagent (Promega). The channel-cloned

vector (2  $\mu$ g) was mixed with 0.5  $\mu$ g of the EGFP-cloned vector in 100 $\mu$ L of the culture medium. Next, 3  $\mu$ L Fugene HD reagent was added and the mixture was incubated for 10 min before the transfection mixture was gently dropped onto cultured cells. After incubation for 16-48 h, the cells were used for electrophysiological measurements. In the measurement of I-V relation curves, the pipette solution contains 75 mM NaF, 40 mM CsF, 35 mM CsCl, 10 mM EGTA, and 10 mM HEPES (pH 7.4 adjusted by CsOH)

For evaluation of ion selectivity, high Na pipette solution (115 mM NaF, 35 mM NaCl, 10 mM EGTA, and 10 mM HEPES (pH 7.4 adjusted by NaOH)) was used. For the evaluation of Ca, Sr, K and Cs selectivity, Ca solution (100 mM CaCl<sub>2</sub>, 10 mM HEPES (pH 7.4 adjusted by Ca(OH)<sub>2</sub>), and 10 mM glucose), Sr solution (100 mM SrCl<sub>2</sub>, 10 mM HEPES (pH 7.4 adjusted by Sr(OH)<sub>2</sub>), and 10 mM glucose), K solution (150 mM KCl, 2mM CaCl<sub>2</sub>, 10 mM HEPES (pH 7.4 adjusted by KOH), and 10 mM glucose), and Cs solution (150 mM CsCl, 2mM CaCl<sub>2</sub>, 10 mM HEPES (pH 7.4 adjusted by CsOH), and 10 mM glucose) were used as the bath solution, respectively.  $E_{rev}$  of high Ca<sup>2+</sup> selective channels were measured under three external solutions containing 144mM NMDG-Cl and 4mM CaCl<sub>2</sub>, 135mM NMDG-Cl and 10mM CaCl<sub>2</sub>, 120mM NMDG-Cl and 20mM CaCl<sub>2</sub> (10mM HEPES pH 7.4 adjusted with HCl). And  $E_{rev}$  of high Ca<sup>2+</sup> selective channels for the calculation of  $P_K/P_{Ca}$  and  $P_{Cs}/P_{Ca}$  were measured under external solutions containing 135mM NMDG-Cl and 10mM CaCl<sub>2</sub> (10mM HEPES pH 7.4 adjusted with HCl) with high K pipette solution (115 mM KF, 35 mM KCl, 10 mM EGTA, and 10 mM HEPES (pH 7.4 adjusted by KOH)) and high Cs pipette solution (115 mM CsF, 35 mM CsCl, 10 mM EGTA, and 10 mM HEPES (pH 7.4 adjusted by CsOH)), respectively.  $E_{rev}$  of NavPp for the calculation of  $P_{Ca}/P_{Na}$  or  $P_{Sr}/P_{Na}$  were measured under external solution containing 50mM NMDG-Cl, 40mM NaCl, 40mM CaCl<sub>2</sub> or SrCl<sub>2</sub> and 10mM HEPES pH 7.4 adjusted with NaOH.  $E_{rev}$  of NavPp for the calculation of  $P_{Cs}/P_{Na}$  was measured under high Cs pipette solution and external solution containing 110mM NMDG-Cl, 40mM NaCl, 3mM CaCl<sub>2</sub> and 10mM HEPES pH 7.4 adjusted with NaOH.

As the pipette solution for measurement of the Ca block effect in NavPp, low Na pipette solution (140 mM CsF, 10 mM NaCl, 10 mM EGTA, and 10 mM HEPES (pH 7.4 adjusted by CsOH)) and high Na pipette solution were used for inward and outward current measurement, respectively. As a bath solution, Ca blocking solution (30 mM NaCl, 120 mM NMDG-Cl, 1.5 mM CaCl<sub>2</sub>, 10 mM HEPES (pH 7.4 adjusted by NaOH) and 10 mM glucose) was used for the 1.5 mM Ca blocking condition. In 10mM Ca blocking condition, a bath solution contains 30 mM NaCl, 105 mM NMDG-Cl, 10 mM CaCl<sub>2</sub>, 10 mM HEPES (pH 7.4 adjusted by NaOH) and 10 mM glucose. And, in each

Ca blocking conditions, 15 mM NMDG-Cl was replaced per 10 mM CaCl<sub>2</sub>. The bath solution was changed using the Dynaflo<sup>®</sup> Resolve system. All experiments were conducted at 25 ± 2°C. All results are presented as mean ± standard error.

### **Calculation of ion selectivity by the GHK equation**

To determine the ion selectivity of each channel, the intracellular solution and extracellular solution were arbitrarily set and the reversal potential at each concentration was measured by giving the ramp pulse of membrane potential. The applied ramp pulse was set to include the reversal potential. In addition, a depolarization stimulus of 2-10 ms was inserted to check whether the behavior of the cell changed for each measurement. As a result,  $P_{Ca}/P_{Na}$  was calculated by substituting the obtained reversal potential ( $E_{rev}$ ) into the expression derived from the GHK equation (42);

$$P_{Ca}/P_{Na} = \frac{-([\text{Na}]_i - [\text{Na}]_o e^{-E_{rev}F/RT})(1 - e^{-2E_{rev}F/RT})}{4([\text{Ca}]_i - [\text{Ca}]_o e^{-2E_{rev}F/RT})(1 - e^{-E_{rev}F/RT})}$$

where  $F$  is Faraday's constant,  $R$  is the Gas constant, and  $T$  is 298.1[K]. The same expression was used for Sr<sup>2+</sup>. The Sr<sup>2+</sup> selectivity ( $P_{Sr}/P_{Na}$ ) was measured in the same way.

Na<sup>+</sup> selectivity against monovalent cations ( $P_M/P_{Na}$ ) was calculated by substituting the obtained reversal potential and  $P_{Ca}/P_{Na}$  into the expression derived from the GHK equation (43):

$$P_M/P_{Na} = \left[ \frac{-4([\text{Ca}]_i - [\text{Ca}]_o e^{-2E_{rev}F/RT})(1 - e^{-E_{rev}F/RT})}{([\text{Na}]_i - [\text{Na}]_o e^{-E_{rev}F/RT})(1 - e^{-2E_{rev}F/RT})} \cdot (P_{Ca}/P_{Na}) - 1 \right] \left[ \frac{([\text{Na}]_i - [\text{Na}]_o e^{-E_{rev}F/RT})}{([\text{M}]_i - [\text{M}]_o e^{-E_{rev}F/RT})} \right]$$

### **References**

1. Hille B (2001) Ion Channels of Excitable Membranes, Third Edition (Sunderland, MA: Sinauer Associates Inc).
2. Catterall W (2000) From ionic currents to molecular mechanisms: the structure and function of voltage-gated sodium channels. *Neuron* 26(1):13–25.
3. Strong M, Chandy KG, Gutman GA (1993) Molecular evolution of voltage-sensitive ion channel genes: on the origins of electrical excitability. *Mol Biol Evol* 10(1):221–42.
4. Rahman T, et al. (2014) Two-pore channels provide insight into the evolution of voltage-gated Ca<sup>2+</sup> and Na<sup>+</sup> channels. *Sci Signal* 7(352):ra109–ra109.
5. Ren D, et al. (2001) A prokaryotic voltage-gated sodium channel. *Science*

- 294(5550):2372–5.
6. Koishi R, Xu H, Ren D, Navarro B (2004) A superfamily of voltage-gated sodium channels in bacteria. *J Biol Chem* 279(10):9532–9538.
  7. Ito M, et al. (2004) The voltage-gated Na<sup>+</sup> channel NaVBP has a role in motility, chemotaxis, and pH homeostasis of an alkaliphilic Bacillus. *Proc Natl Acad Sci* 101(29):10566–10571.
  8. Irie K, et al. (2010) Comparative study of the gating motif and C-type inactivation in prokaryotic voltage-gated sodium channels. *J Biol Chem* 285(6):3685–94.
  9. Shimomura T, Irie K, Fujiyoshi Y (2016) Molecular determinants of prokaryotic voltage-gated sodium channels for recognition of local anesthetics. *FEBS J* 283:2881–2895.
  10. Lee S, Goodchild SJ, Ahern CA (2012) Molecular and functional determinants of local anesthetic inhibition of NaChBac. *Channels (Austin)* 6(5):403–406.
  11. Nagura H, et al. (2010) Evidence for lateral mobility of voltage sensors in prokaryotic voltage-gated sodium channels. *Biochem Biophys Res Commun* 399(3):341–6.
  12. Shimomura T, Irie K, Nagura H, Imai T, Fujiyoshi Y (2011) Arrangement and mobility of the voltage sensor domain in prokaryotic voltage-gated sodium channels. *J Biol Chem* 286(9):7409–7417.
  13. Irie K, Haga Y, Shimomura T, Fujiyoshi Y (2018) Optimized expression and purification of NavAb provide the structural insight into the voltage dependence. *FEBS Lett* 592(2):274–283.
  14. Irie K, Shimomura T, Fujiyoshi Y (2012) The C-terminal helical bundle of the tetrameric prokaryotic sodium channel accelerates the inactivation rate. *Nat Commun* 3:793.
  15. Tsai CJ, et al. (2013) Two alternative conformations of a voltage-gated sodium channel. *J Mol Biol* 425(22):4074–4088.
  16. Yue L, Navarro B, Ren D, Ramos A, Clapham DE (2002) The cation selectivity filter of the bacterial sodium channel, NaChBac. *J Gen Physiol* 120(6):845.
  17. Lin CW, et al. (2010) Genetically Increased Cell-Intrinsic Excitability Enhances Neuronal Integration into Adult Brain Circuits. *Neuron* 65(1):32–39.
  18. Bando Y, et al. (2016) Control of Spontaneous Ca<sup>2+</sup> Transients Is Critical for Neuronal Maturation in the Developing Neocortex. *Cereb Cortex* 26(1):106–117.
  19. Kamiya A, et al. (2019) Genetic manipulation of autonomic nerve fiber innervation and activity and its effect on breast cancer progression. *Nat Neurosci*.



- doi:10.1038/s41593-019-0430-3.
20. Tang L, et al. (2013) Structural basis for Ca<sup>2+</sup> selectivity of a voltage-gated calcium channel. *Nature* 505(7481):56–61.
  21. Tang L, et al. (2016) Structural basis for inhibition of a voltage-gated Ca<sup>2+</sup> channel by Ca<sup>2+</sup> antagonist drugs. *Nature* 537(7618):117–121.
  22. Tang L, et al. (2014) Structural basis for Ca<sup>2+</sup> selectivity of a voltage-gated calcium channel. *Nature* 505(7481):56–61.
  23. Heinemann SH, Terlau H, Stühmer W, Imoto K, Numa S (1992) Calcium channel characteristics conferred on the sodium channel by single mutations. *Nature* 356(6368):441–443.
  24. Almers W, McCleskey EW (1984) Non-selective conductance in calcium channels of frog muscle: calcium selectivity in a single-file pore. *J Physiol* 353(1):585–608.
  25. Finol-Urdaneta RK, et al. (2014) Sodium channel selectivity and conduction: prokaryotes have devised their own molecular strategy. *J Gen Physiol* 143(2):157–71.
  26. Wu J, et al. (2016) Structure of the voltage-gated calcium channel Cav1.1 at 3.6 Å resolution. *Nature* 537(7619):191–196.
  27. Domínguez DC, Guragain M, Patrauchan M (2015) Calcium binding proteins and calcium signaling in prokaryotes. *Cell Calcium* 57(3):151–165.
  28. Dominguez DC (2004) Calcium signalling in bacteria. *Mol Microbiol* 54(2):291–297.
  29. ORDAL GW (1977) Calcium ion regulates chemotactic behaviour in bacteria. *Nature* 270(5632):66–67.
  30. Tisa LS, Adler J (1995) Cytoplasmic free-Ca<sup>2+</sup> level rises with repellents and falls with attractants in *Escherichia coli* chemotaxis. *Proc Natl Acad Sci U S A* 92(23):10777–81.
  31. Tisa LS, Olivera BM, Adler J (1993) Inhibition of *Escherichia coli* chemotaxis by omega-conotoxin, a calcium ion channel blocker. *J Bacteriol* 175(5):1235–1238.
  32. Loginova LG, Egorova LA [Thermus ruber obligate thermophilic bacteria in the thermal springs of Kamchatka]. *Mikrobiologiya* 44(4):661–5.
  33. Iizuka T, et al. (2003) *Plesiocystis pacifica* gen. nov., sp. nov., a marine myxobacterium that contains dihydrogenated menaquinone, isolated from the Pacific coasts of Japan. *Int J Syst Evol Microbiol* 53(1):189–195.
  34. DeCaen PG, Takahashi Y, Krulwich T a, Ito M, Clapham DE (2014) Ionic

- selectivity and thermal adaptations within the voltage-gated sodium channel family of alkaliphilic *Bacillus*. *Elife* 3:1–15.
35. Helliwell KE, et al. (2019) Alternative Mechanisms for Fast Na<sup>+</sup>/Ca<sup>2+</sup> Signaling in Eukaryotes via a Novel Class of Single-Domain Voltage-Gated Channels. *Curr Biol* 29(9):1503-1511.e6.
  36. Zalk R, et al. (2015) Structure of a mammalian ryanodine receptor. *Nature* 517(7532):44–49.
  37. Yan Z, et al. (2015) Structure of the rabbit ryanodine receptor RyR1 at near-atomic resolution. *Nature* 517(7532):50–55.
  38. Halling DB, Liebeskind BJ, Hall AW, Aldrich RW (2016) Conserved properties of individual Ca<sup>2+</sup>-binding sites in calmodulin. *Proc Natl Acad Sci* 113(9):E1216–E1225.
  39. Yu FH, Catterall WA (2004) The VGL-kanome: a protein superfamily specialized for electrical signaling and ionic homeostasis. *Sci STKE* 2004(253):re15.
  40. Darszon A, Nishigaki T, Beltran C, Treviño CL (2011) Calcium Channels in the Development, Maturation, and Function of Spermatozoa. *Physiol Rev* 91(4):1305–1355.
  41. Tateyama M, Kubo Y (2018) Gi/o-coupled muscarinic receptors co-localize with GIRK channel for efficient channel activation. *PLoS One* 13(9):1–18.
  42. Frazier CJ, George EG, Jones SW (2000) Apparent change in ion selectivity caused by changes in intracellular K<sup>(+)</sup> during whole-cell recording. *Biophys J* 78(4):1872–80.
  43. Lopin K V., Thevenod F, Page JC, Jones SW (2012) Cd<sup>2+</sup> Block and Permeation of CaV3.1 (α1G) T-Type Calcium Channels: Candidate Mechanism for Cd<sup>2+</sup> Influx. *Mol Pharmacol* 82(6):1183–1193.

### **Acknowledgements**

We very appreciate to Dr. Yoshihiro Kubo for the critical suggestion about the structure of our manuscript. This work was supported by Grants-in-Aid for Scientific Research (S), a Grant-in-Aid for Young Scientists (B), the Japan Agency for Medical Research and Development and the Toyoaki Scholarship Foundation.

### **Author contribution**

T.S. and K.I. conducted the experiments; T.S. searched for homologues; Y.Y. and K.I. performed the electrophysiological experiments of insect cells; M.T. performed the electrophysiological experiments of mammalian cells; T.S., Y.Y., H.N. and K.I. optimized the measurement conditions; T.S., Y.Y., H.N., Y.F. and K.I. contributed to the study design and wrote the paper.

## **Figure legends.**

### **Table1. Relative permeability of CavMr and NavPp**

#### **Figure 1. Sequence analysis and the representative current recordings of the novel BacNav homologues**

a). Phylogenetic tree of the BacNav homologues with their GenBank<sup>TM</sup> accession numbers. The ClustalW program was used to align the multiple protein sequences of the BacNav homologues. The phylogenetic tree was generated using “PROTDIST”, one of the PHYLIP package (Phylogeny Inference Package: <http://evolution.genetics.washington.edu/phylip.html>). The branch lengths are proportional to the sequence divergence, with the scale bar corresponding to 0.1 substitution per amino acid position. Four homologues colored that are not included in canonical BacNavs were cloned and expressed to check the current activity. Those of two which are underlined in red and shown as bold generated the detectable currents. b). Schematic secondary structure and selectivity filter sequence of BacNavs and human Cavs. Cylinder indicates  $\alpha$ -helix. The selectivity filter sequences are indicated by alphabetical characters. Negatively charged residues are colored by red. Glycine residues in the position 4 are colored by cyan. The straight lines indicate the other part of pore domain. The selectivity filter sequence of hCav1.1 (UniProt ID: Q13698), hCav2.1 (O00555) and hCav3.1 (O43497), were used. c and d). Representative current traces to obtain the current-voltage relationships of CavMr (c) and NavPp (d) in Sf9 cells. The straight lines indicating the zero-current level in the representative current traces. Currents were generated under the bath solutions containing high Na<sup>+</sup> (top) and high Ca<sup>2+</sup> (middle), by a series of step-pulses shown in bottom. e and f). Current-voltage relationships of CavMr (e) and NavPp (f) measured under the different bath solutions (filled black; 150 mM NaCl, open black; 75 mM NaCl and 75 mM NMDG-HCl, open red; 75 mM NaCl and 50 mM CaCl<sub>2</sub>, filled red; 50 mM CaCl<sub>2</sub> and 75 mM NMDG-HCl). Currents of CavMr and NavPp were normalized to that by 0mV depolarization stimuli under 75 mM NaCl and 50 mM CaCl<sub>2</sub> bath solution and 150 mM NaCl bath solution, respectively.

#### **Figure 2. Cation selectivity of CavMr**

a and b). Recordings of the reversal potential of CavMr currents using the ramp protocol. Currents were generated by the step pulse of -20 mV from -140 mV holding potential, followed by the ramp pulses with different voltage values (shown at the bottom of

panels a and b). The values of the reversal potential recorded with three different ramp pulses were averaged. Currents were measured under the bath solution containing 4 mM (a) and 10 and 20 mM (b)  $\text{CaCl}_2$  and the pipette solution with 150 mM NaCl. c). The plot of the reversal potential to the bath  $[\text{Ca}^{2+}]_{\text{out}}$ . Each value was obtained using the protocol shown in a and b. The relationship was fitted by a line with the slope of  $41.07 \pm 2.64$  mV per decade ( $n = 4$ ). d). Representative current traces to obtain the reversal potential under the condition of 100 mM  $[\text{Sr}^{2+}]_{\text{out}}$  and 150 mM  $[\text{Na}^+]_{\text{in}}$ . Currents were generated by the protocol shown in the lower part. e). Representative current traces to investigate the  $P_{\text{Cs}}/P_{\text{Ca}}$  and  $P_{\text{K}}/P_{\text{Ca}}$ , the pipette solutions contained 150 mM  $[\text{Cs}^+]_{\text{in}}$  for  $P_{\text{Cs}}/P_{\text{Ca}}$  and 150 mM  $[\text{K}^+]_{\text{in}}$  for  $P_{\text{K}}/P_{\text{Ca}}$ , while the bath solution contained 10 mM  $[\text{Ca}^{2+}]_{\text{out}}$  in both cases. f). The relative permeability of  $\text{Ca}^{2+}$  or  $\text{Sr}^{2+}$  to  $\text{Na}^+$  in CavMr, calculated from the reversal potential that was obtained in a, b, and d. g). The relative permeability of each monovalent cation to  $\text{Ca}^{2+}$  in CavMr, derived from the data shown in e.

### **Figure 3. $\text{Na}^+$ permeability and the extracellular $\text{Ca}^{2+}$ -dependent inhibition in NavPp**

a)  $[\text{Ca}^{2+}]_{\text{out}}$  dependent inhibitory effects in NavPp. Currents were normalized to those under 1.5 mM  $[\text{Ca}^{2+}]_{\text{out}}$  (filled square; NavAb current in the 30 mM  $[\text{Na}^+]_{\text{out}}$  and 10 mM  $[\text{Na}^+]_{\text{in}}$  (representative data are shown in Fig. S3b), open triangle down; NavPp inward current in the 30 mM  $[\text{Na}^+]_{\text{out}}$  and 10 mM  $[\text{Na}^+]_{\text{in}}$  (Fig. S3a), open triangle up; NavPp outward current in the 30 mM  $[\text{Na}^+]_{\text{out}}$  and 150 mM  $[\text{Na}^+]_{\text{in}}$  (Fig. S3c), filled triangle up; NavPp outward current in the 0 mM  $[\text{Na}^+]_{\text{out}}$  and 150 mM  $[\text{Na}^+]_{\text{in}}$ . b). Representative currents to obtain the reversal potential in NavPp for  $P_{\text{Ca}}/P_{\text{Na}}$ . Currents were generated by the ramp protocol shown in bottom.  $[\text{Ca}^{2+}]_{\text{out}}$  was varied from 10 to 60 mM with the fixed  $[\text{Na}^+]$  both in the bath (60mM) and pipette (150mM). c). Representative currents to obtain the reversal potential in NavPp for  $P_{\text{Sr}}/P_{\text{Na}}$ . Currents were generated by the ramp protocol shown in bottom.  $[\text{Sr}^{2+}]_{\text{out}}$  was 40 mM with the fixed  $[\text{Na}^+]$  both in the bath (40mM) and pipette (150mM). d). The relative permeability of different cation species to  $\text{Na}^+$  in NavPp, calculated from the reversal potential that was obtained in b, c and Fig.S3d and e.

### **Figure 4. The cation selectivity of the swapped mutant channels in their selectivity filter between CavMr and NavPp**

a) Amino acid sequences of the selectivity filter in the swapped mutants, CavMr-Pp, Nav-Pp, NavAb\_Mr, and CavMr\_Ab. The selectivity filter sequences of CavMr, and

NavPp, and NavAb are indicated by alphabetical characters with cyan, red, and gray shade, respectively. Negatively charged residues are colored by red. Glycine residues are colored by cyan. The straight lines of cyan, red, and black indicates the other part of pore domain of CavMr, NavPp, and NavAb, respectively. b) Pore domains of crystal structure of NavAb (PDB code:5YUA). The selectivity filter, which corresponds to the sequences shown in a, was indicated in red. c) The relative permeability of divalent cations to Na<sup>+</sup> (left) and that of monovalent cations to Ca<sup>2+</sup> (right) in NavPp-Mr. d) The relative permeability of different cation species to Na<sup>+</sup> in CavMr-Pp.

**Figure 5. The single point mutations losing and obtaining Ca<sup>2+</sup> selectivity of CavMr and NavPp, respectively.**

a) The relative permeability of each cation species to Na<sup>+</sup> in the single-point mutants of CavMr. The selectivity filter of CavMr was changed to the corresponding residues of NavPp at position 4 (G4D) and position 6 (V6T), respectively b) The relative permeability of each cation species to Na<sup>+</sup> in the G4S mutants of CavMr, whose position 4 residue of the selectivity filter was mutated to the corresponding residue of canonical BacNavs. c) The relative permeability of each cation species to Na<sup>+</sup> in the single-point mutants of NavPp. The selectivity filter of NavPp was changed to the corresponding residues of CavMr at position 4 (D4G) and position 6 (T6V), respectively.

**Figure 6. Comparison between mammalian and prokaryotic Cav.**

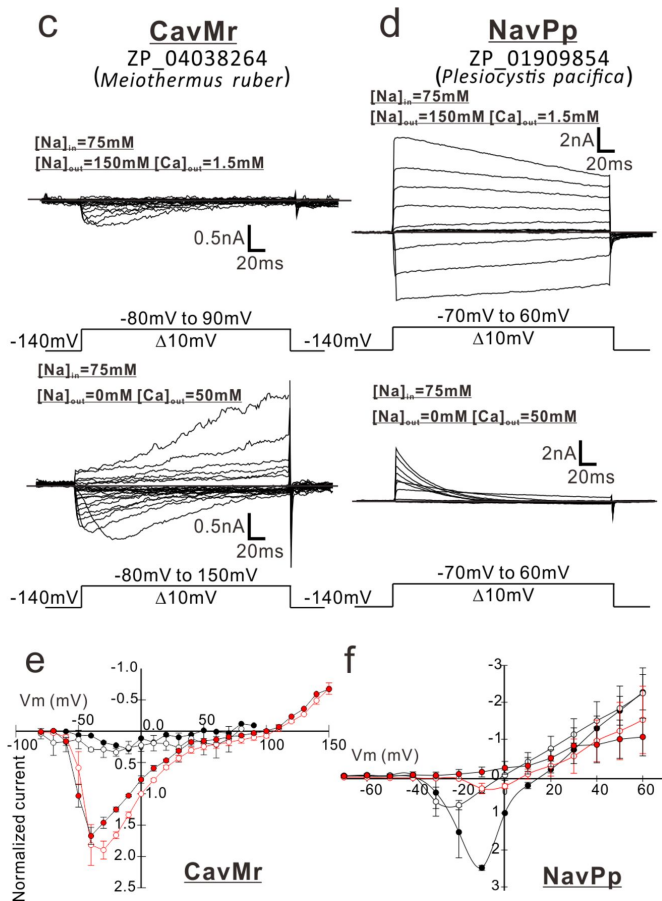
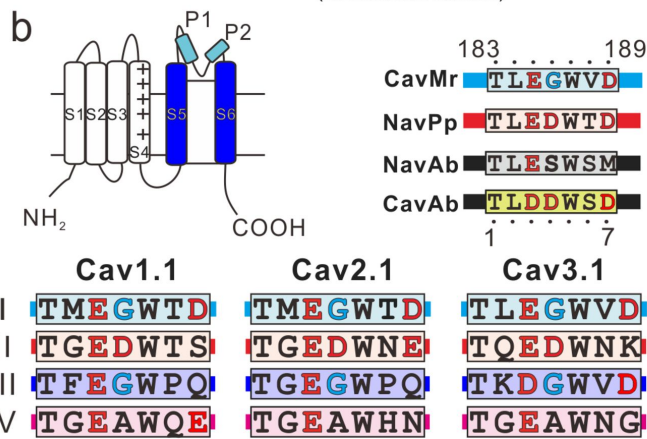
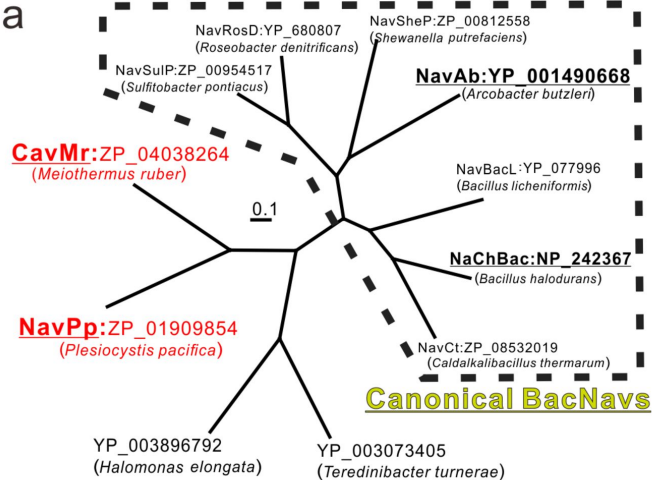
a and b). Structures of the selectivity filter in CavAb (PDB code: 4MVZ) and NavAb (PDB code: 5YUA). c and d) Structure of the rabbit Cav1.1 selectivity filter (PDB code: 5GJV). The subdomains I and III (c), and II and IV (d) were separately shown. The carbon atoms of negatively charged residues were indicated in pink. Dashed green circle indicates the wide entrance of the selectivity filter.

	$P_{Ca}/P_{Na}$	$P_{Sr}/P_{Na}$	$P_{K}/P_{Na}$	$P_{Cs}/P_{Na}$
CavMr G240A	218 ± 38 (n= 20 )	40.6 ± 3.4 (n= 6 )	0.0036±0.00072 <sup>a</sup> (n= 4 )	0.0021±0.00042 <sup>b</sup> (n= 4 )
Pp	13.8 ± 2.0 (n= 7 )	24.5 ± 0.3 (n= 5 )	0.95 ± 0.04 (n= 4 )	0.57 ± 0.05 (n= 3 )
G4D	7.73 ± 2.24 (n= 11 )	18.6 ± 6.1 (n= 4 )	1.20 ± 0.28 (n= 4 )	0.87 ± 0.21 (n= 4 )
G4S	11.9 ± 1.5 (n= 5 )	4.23 ± 0.27 (n= 5 )	1.54 ± 0.12 (n= 5 )	2.02 ± 0.48 (n= 3 )
V6T	40.1 ± 9.7 (n= 5 )	13.3 ± 2.5 (n= 5 )	0.69 ± 0.26 (n= 3 )	0.54 ± 0.60 (n= 3 )
D7M	144 ± 12 (n= 5 )	20.7 ± 2.7 (n= 5 )	N.D.	N.D.
NavPp T232A	0.308±0.028 (n= 10 )	0.38±0.027 (n= 9 )	0.16±0.026 (n= 9 )	0.0052±0.0006 (n= 7 )
Mr	215 ± 33 (n= 7 )	86.3 ± 12.2 (n= 4 )	0.0045±0.00072 <sup>a</sup> (n= 4 )	0.0135±0.0039 <sup>b</sup> (n= 9 )
D4G	41.4 ± 6.7 (n= 10 )	8.85 ± 0.95 (n= 4 )	<< 0.01 (n= 3 )	<< 0.01 (n= 4 )
D4S	1.49 ± 0.18 (n= 6 )	0.47 ± 0.08 (n= 6 )	0.24 ± 0.01 (n= 4 )	0.11 ± 0.02 (n= 3 )
T6V	1.72 ± 0.19 (n= 10 )	33.9 ± 5.0 (n= 8 )	0.99 ± 0.03 (n= 4 )	0.84 ± 0.02 (n= 4 )

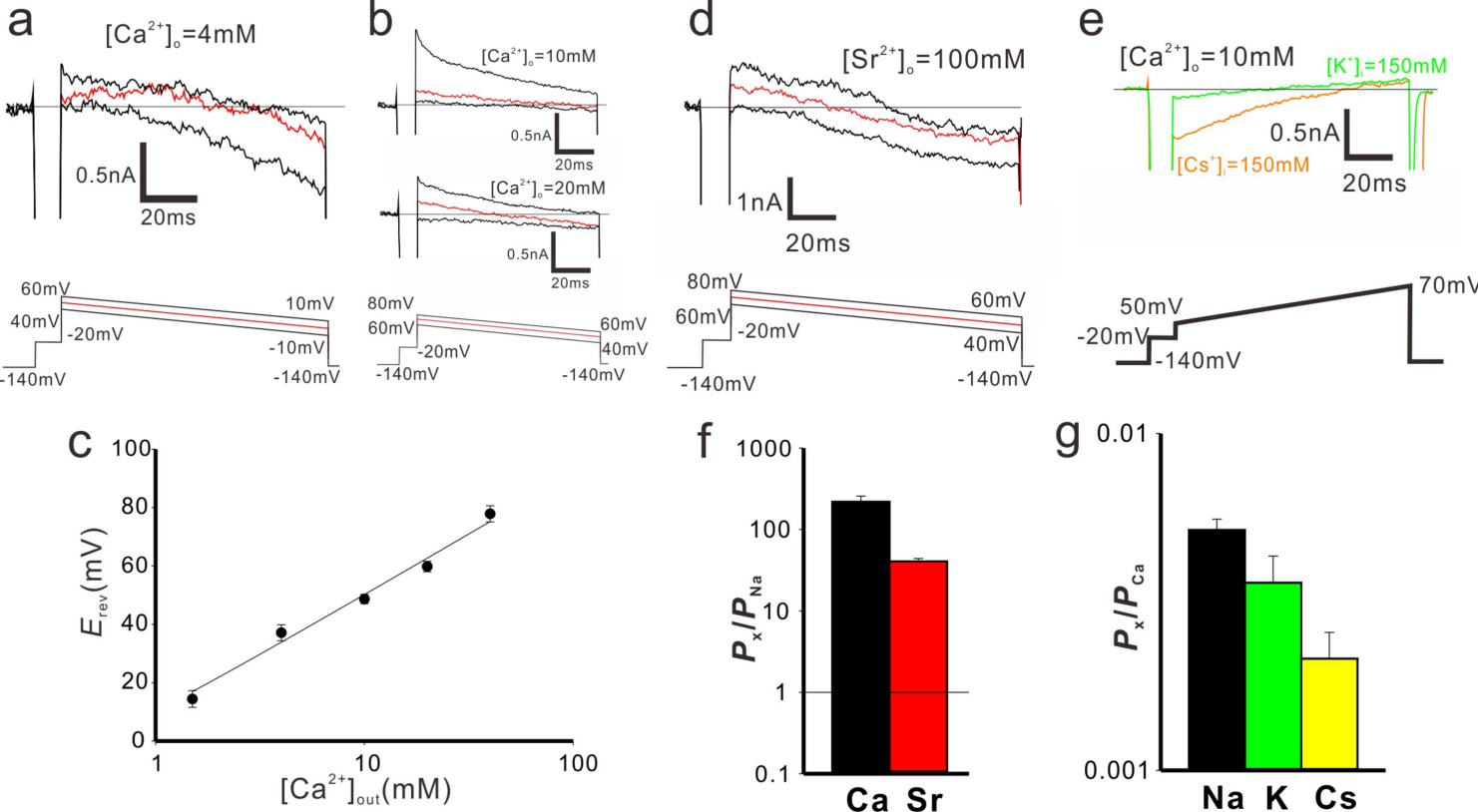
**Table1. Relative permeability of CavMr and NavPp**

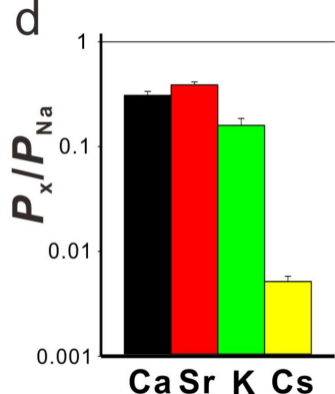
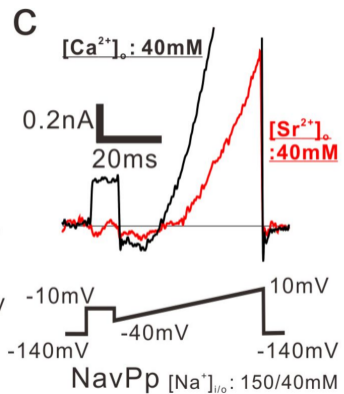
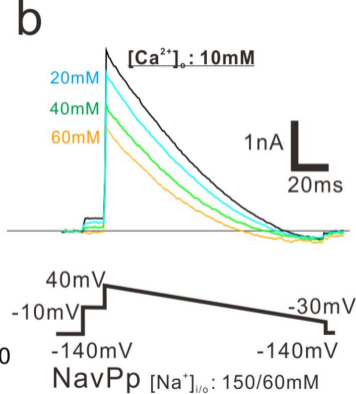
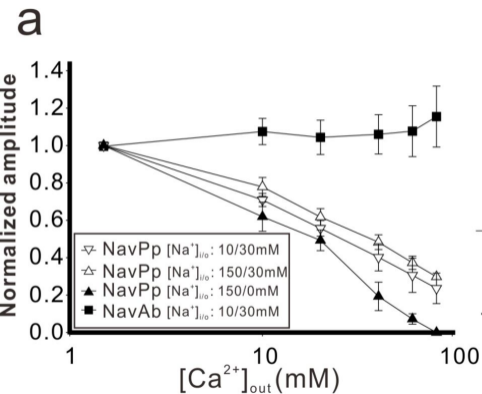
<sup>a</sup> Because of high Ca<sup>2+</sup> selectivity,  $P_K/P_{Ca}$  were indicated

<sup>b</sup> Because of high Ca<sup>2+</sup> selectivity,  $P_{Cs}/P_{Ca}$  were indicated

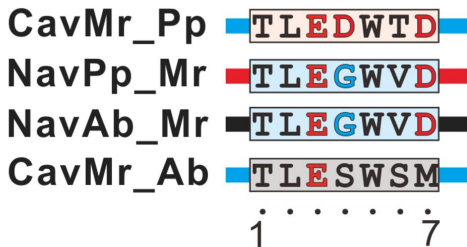




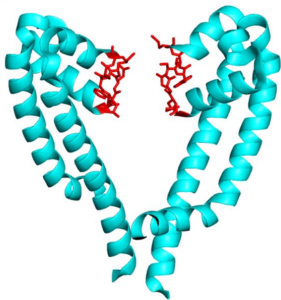




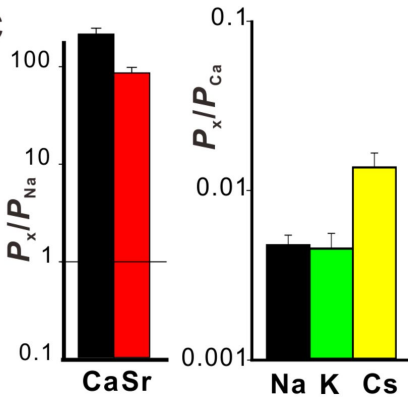
a



b

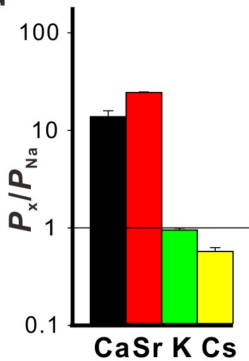


c

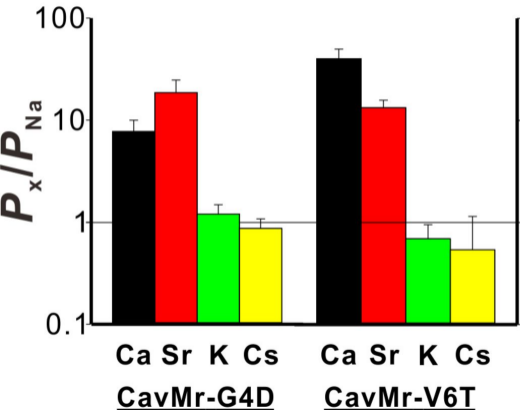
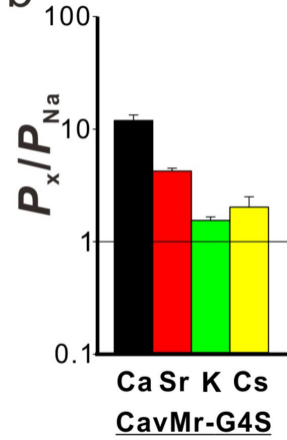
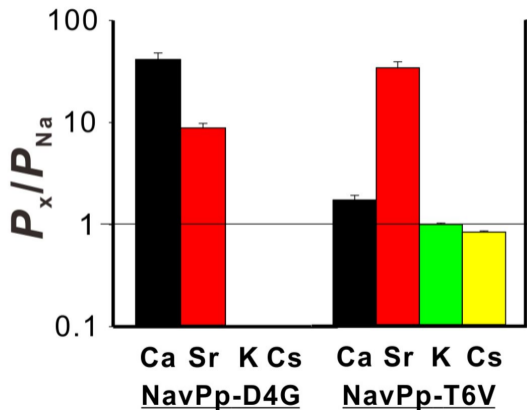


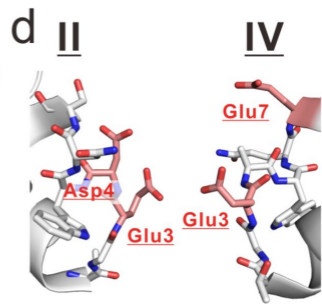
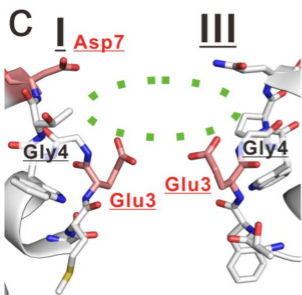
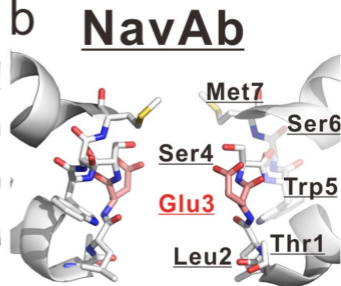
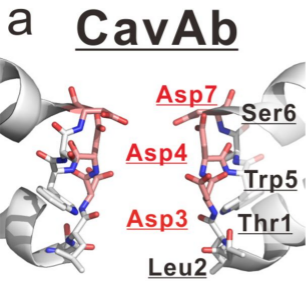
NavPp-Mr

d



CavMr-Pp

**a****b****c**



I 1-TMEGWTD-7

II 1-TGEDWNS-7

III 1-TFEGWPQ-7

IV 1-TGEAWQE-7

Cav1.1